Magnetic Resonance in Medicine 43:739–746 (2000)

Cerebral Perfusion and Arterial Transit Time Changes During Task Activation Determined With Continuous Arterial Spin Labeling

Julio B. Gonzalez-At, David C. Alsop,* and John A. Detre

Perfusion imaging by arterial spin labeling (ASL) can be highly sensitive to the transit time from the labeling site to the tissue. We report the results of a study designed to separate the transit time and perfusion contributions to activation in ASL images accompanying motor and visual stimulation. Fractional transit time decreases were found to be comparable to fractional perfusion increases and the transit time change was found to be the greatest contributor to ASL signal change in ASL sequences without delayed acquisition. The implications for activation imaging with ASL and the arterial control of flow are discussed. Magn Reson Med 43:739–746, 2000. © 2000 Wiley-Liss, Inc.

Key words: cerebral blood flow; arterial transit time; visual cortex; motor cortex; activation

Arterial spin labeling (ASL) techniques are capable of quantifying regional tissue perfusion noninvasively. Magnetic resonance imaging of regional brain activation imaging using ASL provides several potential benefits over blood oxygenation sensitive (BOLD) techniques that make its pursuit desirable. Because ASL techniques provide a diffusible tracer, cerebral blood flow (CBF) changes can be measured in physiologically relevant units (mL·100 g^{-1}·min^{-1}), which are directly analogous to measurements obtained using ^{15}O-PET scanning (1,2). In contrast to BOLD activation studies, this allows both resting and activated perfusion to be quantified, an advantage that may be particularly important for meaningful interpretation of studies in clinical populations. Further, because ASL perfusion contrast is based upon longitudinal magnetization, imaging can be performed with pulse sequences, such as RARE or GRASE (3,4), that are insensitive to the bulk susceptibility effects that can degrade BOLD studies in certain brain regions. ASL images can be interleaved with control images to reduce long term instabilities in the image intensity (5). Finally, ASL activation may be better localized in brain parenchyma than BOLD signal changes since the 'tracer' is diffusible.

A number of groups have reported successful detection of focal activation using pulsed ASL (6–9) or continuous ASL (CASL) (10,11) perfusion contrast. Although each of these studies has shown task-specific focal signal changes, the influences of data acquisition parameters were not systematically examined. In particular, ASL techniques are highly sensitive to changes in arterial transit time (9,12), which must be considered in the optimization and quantification of ASL activation studies. The purpose of this study was to characterize changes in both perfusion and arterial transit time (ATT) during task activation using CASL.

In general, the effect of ASL on distal image intensity is dependent upon both perfusion and transit time from the tagging plane to the imaging slice (9,12,13). For the case of CASL, the introduction of a sufficiently long delay between the end of labeling and the start of image acquisition reduces the image dependence on transit time (12). When multiple images are acquired with different delays, both perfusion and transit time can be measured. Below we report the results of a multiple delay study of CASL activation in response to simultaneous motor and visual stimulation. This task allowed alterations in perfusion and transit time to be measured in brain regions supplied by both the anterior and posterior vascular distributions.

THEORY

The previously derived (12) expression for the signal intensity in CASL images with post-labeling delay, w, is

$$\Delta M \equiv \frac{2\alpha M_b^0 f}{\lambda}\left\{ T_{1ns}\exp\left(\frac{-\delta}{T_{1a}}\right)\left[\exp\left(\frac{\min(\delta - w, 0)}{T_{1ns}}\right) - \exp\left(\frac{-w}{T_{1ns}}\right)\left(1 - \frac{T_{1s}}{T_{1ns}}\right)\right] + T_{1a}\left[\exp\left(\frac{\min(\delta_a - w, 0) - \delta_a}{T_{1a}}\right) - \exp\left(\frac{\min(\delta - w, 0) - \delta}{T_{1a}}\right)\right]\right\} \quad [1]$$

where α is the inversion efficiency (14), M_b^0 is the equilibrium brain tissue magnetization, f is the blood flow in [ml·g^{-1}·s^{-1}], λ is the brain-blood partition coefficient (defined as [ml of water per gram of tissue/ml of water per ml of blood]), T_{1s} and T_{1ns} are the effective time constants for the longitudinal magnetization (T_{1app} (13)) with and without the magnetization transfer saturation effect due to the off-resonance inversion power applied, δ is the transit time from the labeling plane to the tissue in the slice imaged, T_{1a} is the T_1 of arterial blood and δ_a is the transit time from the labeling plane to the arterial vascular compartment.

The model considers contributions from two compartments. The first term inside the curly brackets in Eq. [1] describes the contribution from the tissue compartment

Departments of Neurology and Radiology, University of Pennsylvania, Philadelphia, Pennsylvania.

Grant sponsor: National Institute of Neurological Disorders and Stroke; Grant numbers: NS01668; NS02079; Grant sponsor: Whitaker Foundation.

*Correspondence to: David C. Alsop, Department of Radiology, University of Pennsylvania Medical Center, 3400 Spruce Street, Philadelphia, PA 19104-4283. E-mail: alsop@oasis.rad.upenn.edu

Received 20 January 1999; revised 6 December 1999; accepted 19 January 2000.

while the second term describes the contribution from the vascular compartment to the total intensity of the pixel.

Implicit in Eq. [1] is the assumption of unique transit times from the tagging plane to the imaging plane. In reality, several effects may invalidate this assumption, such as the possibility of several arterial trajectories supplying the same activated region, different trajectories supplying different parts of the activated region, or the likely effect of a spread in the velocity at which the blood travels through the cross section of the carotid and vertebral arteries. Usually blood flows much more slowly near the wall of the vessel than near the center due to laminar flow effects.

To assess the effect of a spread in transit times on the observed signal, we developed a model for the distribution of transit times assuming that no mixing of blood traveling at different distances from the vessel wall occurs. Because some mixing is bound to occur at vessel branches, this model represents the most extreme case of spreading. When the flow is laminar, the fraction of the blood flow through a vessel carried by blood traveling at a velocity between v and $v + dv$ is given by (14)

$$p(v) = \frac{2v}{v_{\max}^2} \quad 0 < v < v_{\max}\,. \qquad [2]$$

The transit time through the vessel is inversely proportional to the velocity. Assuming that the position of blood relative to the vessel wall is maintained throughout the multiple branches of the vascular tree, the total transit time will also be inversely proportional to velocity. The distribution of transit times can then be derived from the distribution of velocities in Eq. [2],

$$p(\delta) = \frac{2\delta_{\min}^2}{\delta^3} \quad \delta > \delta_{\min}\,. \qquad [3]$$

Thus, the signal will be obtained by averaging over all possible transit times as

$$\langle \Delta M \rangle \equiv \int_{\langle \delta_a \rangle/2}^{\infty} \frac{2\delta_{\min}^2}{\delta^3} d\tau \Delta M \qquad [4]$$

with ΔM given by Eq. [1]. The lower limit of $\langle \delta_a/2 \rangle$ comes from the relation

$$\langle \delta_a \rangle = \int_{\delta_{\min}}^{\infty} \frac{2\delta_{\min}^2}{\delta^3} d\delta\delta = 2\delta_{\min}\,.$$

In our analysis of experimental results, we fit our data to both the single transit time model described by Eq. [1] and the model with the transit distribution described by Eq. [4]. Because these two distributions represent the extreme cases of perfect mixing and no mixing of blood traveling at different velocities, comparison of the results using the two different models will test the sensitivity of the results to the shape of the transit time distribution.

METHODS

All images were acquired with a 1.5 Tesla GE Signa scanner (GE Medical Systems, Milwaukee, WI) using the standard head RF coil. ASL images were obtained from eight axial slices using flow driven adiabatic inversion (15) CASL and gradient echo echoplanar imaging. A field of view (FOV) of 24 × 15 cm, an acquisition matrix of 64 × 40, a slice thickness of 8 mm, an interslice gap of 2 mm, a TR of 4 sec, and a TE of 22 msec were selected. Labeling was performed with a 0.25 G/cm gradient and 35 mG RF irradiation applied 8 cm beneath the center of acquired slices, which placed the labeling plane 4.5 cm below the lowest slice (10). Interleaved images with (labeled) and without (control) labeling were taken while controlling for off-resonance effects by applying an amplitude modulated version of the labeling pulse (16). Acquisition of each slice required 60 msec and the images were acquired sequentially, the last slice being acquired 420 msec after the first one.

Following routine T_1-weighted anatomical imaging and fast T_1 mapping (12), each of the six subjects underwent five task activation scans lasting eight minutes. Each scan was identical except they were acquired with different post-labeling delays of 100, 300, 600, 900, and 1200 msec. The order of the delays was varied among subjects to control for systematic effects due to fatigue or habituation to the task. During each scan, 60-sec periods of rest and activation were interleaved starting with a period of rest. A total of 60 label minus control multislice image pairs were acquired per run. The activation task consisted of visual stimulation using LED goggles flashing at 10 Hz and simultaneous bilateral self-paced finger opposition.

Averages of the difference between control and labeled images were separately computed for the resting and activated periods within a run. Each of these ASL difference images was corrected for subject motion by using an algorithm based on a principal component analysis of the control images taken during the resting periods (17). Difference images at rest were then subtracted from difference images during the stimulation period to obtain activation images for each subject (see Figs. 1 and 2). The images obtained for the 100-msec post-labeling delay were used to manually define three regions of interest (ROIs) for each of the subjects, because the shorter delay images provided the best signal-to-noise ratio. Regions corresponding to activation in calcarine cortex and both left and right motor cortices were drawn. Within these regions only pixels whose T_{1ns} (T_1 of brain tissue without saturation effects from the CASL pulse), as determined by the procedure described in Alsop and Detre (12), was greater than 900 msec were kept for further analysis. These pixels restricted the subject ROI mainly to gray matter, which helped to reduce noise by eliminating pixels that should not activate as robustly. We avoided the use of statistical tests to define the ROIs based on a significance threshold as this could introduce a bias in our analysis.

The average ASL difference signal within each region was computed for each subject. The sequential acquisition of slices at a rate of one image per 60 msec means that the post-labeling delay was not identical for each slice. Slices were acquired in an interleaved ascending order: 1, 3, 5, 7,

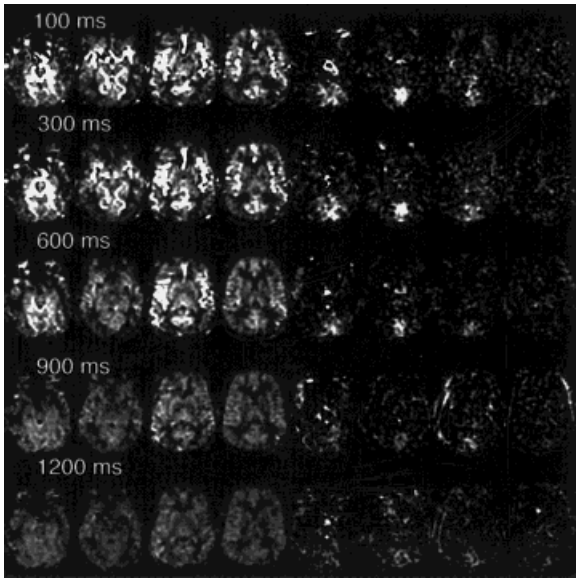

FIG. 1. Effects of post-labeling delay on ASL signal in visual cortex. ASL images in the resting state from one volunteer (four leftmost columns) and the corresponding activation images (four rightmost columns) for post-labeling delays of 100, 300, 600, 900, and 1200 msec are shown. Bright vascular features evident in the resting ASL images at short delays are clearly diminished at longer delays. In contrast, the activation images do not contain bright vessels and the spatial distribution of the activation does not change significantly with delay.

2, 4, 6, and 8 where the numbers represent position relative to the most inferior slice. This interleaving complicated our analysis since neighboring slices differed in post-labeling delay by 240 msec. Variations between subjects in the specific slices where activation was detected and the existence of activation spread across several slices caused a distribution of post-labeling delays for the voxels within each ROI. To take these effects into consideration we computed the mean time between labeling and acquisition for each ROI in each subject. The spread in acquisition times of the different slices also makes it possible that the RF excitation pulse used to image an earlier slice will saturate blood destined to flow into another slice before it is imaged. Such saturation of the labeled blood would artificially decrease the ASL signal intensity in the second slice. Nevertheless, we argue in the Appendix that this label saturation effect in our study should cause a change in ASL signal intensity of less than 10% and should not affect the significant conclusions of the study.

Individual subject resting and activated ASL signal for motor and visual cortex were fit to the two models for ASL signal, the single transit time and distributed transit time models, using a nonlinear least squares algorithm to extract an amplitude (proportional to the perfusion) and the ATT (δ_a). We also created a pseudo-subject data set by averaging the subjects' ROI values normalized by the resting perfusion amplitude resulting from the individual fits. The mean delay for each pseudo-subject data point was calculated by averaging the mean delays calculated for each subject. These pseudo-subject data were also fit to the two models described above.

The values of T_{1ns}, T_{1s}, and T_{1a} used for the fits were taken from a previous publication (12) (T_{1ns} = 1151 msec, T_{1s} = 746 msec, T_{1a} = 1100 msec) and are consistent with other literature values (18–21). There is some disagreement in the literature over the T_1 of blood at 1.5 Tesla, but setting T_{1a} = 1300 msec produced only a 10% change in the fitted values and did not alter our basic conclusions. In gray matter, where activation occurs, the T_1 of tissue and blood are very similar. Under these conditions, the signal intensity becomes insensitive to the tissue transit time, δ, and is primarily determined by δ_a and the post-labeling delay, w. Thus, we set δ = 2000 msec. Changing δ to 1400 msec produced only a small variation of 2% in the fitted values.

The fitted transit times and fractional perfusion change for each subject were tabulated and the significance of the change from resting to activated state were assessed with a paired t-test. Because the individual subject data may also contain habituation effects, the individual subject statistics are probably overly conservative.

The different relative positions of the measuring slices and the labeling plane result in a small variation of T_{1s} with the slice number. To determine the magnitude of this effect we have varied the value of T_{1s} used for the fits over a range from 600 to 1200 msec. The total change in the fitted transit time values was less than 5%.

RESULTS

Resting ASL difference images (leftmost images in Figs. 1 and 2) demonstrated the expected effects of varying the

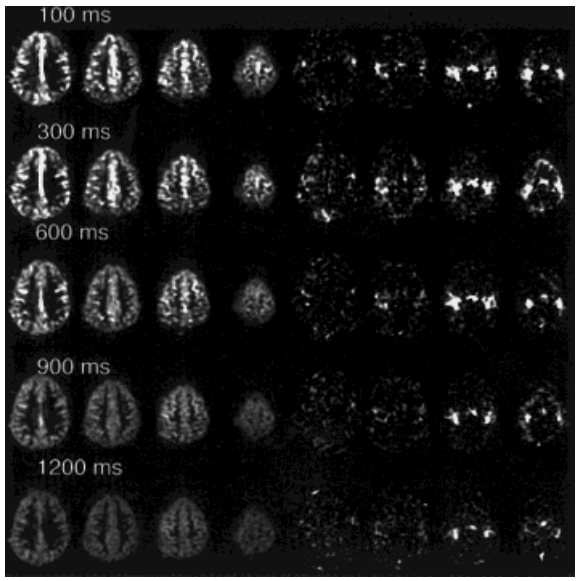

FIG. 2. Effects of post-labeling delay on ASL signal in motor cortex. ASL images in the resting state from one volunteer (four leftmost columns) and the corresponding activation images (four rightmost columns) for post-labeling delays of 100, 300, 600, 900, and 1200 msec are shown. Bright vascular features evident in the resting ASL images at short delays are clearly diminished at longer delays. In contrast, the activation images do not contain bright vessels and the spatial distribution of the activation does not change significantly with delay.

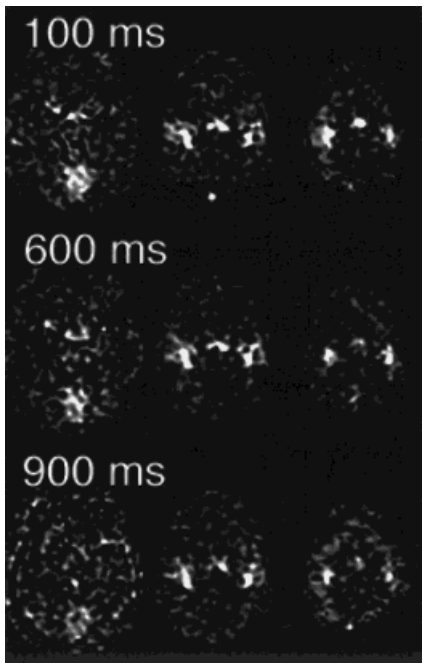

FIG. 3. The spatial distribution of visual (leftmost column) and motor (two rightmost columns) activation for three post-labeling delays. The images are scaled to compensate for the delay dependence of the intensity predicted by Eq. [1].

post-labeling delay. Images acquired with shorter post-labeling delays demonstrated brighter signal but much of it appeared as bright linear and point-like features, which likely result from arteries containing labeled blood; in the most inferior slices of Fig. 1, the circle of Willis and the major cerebral arteries are readily identified. As the post-labeling delay was increased, the bright vascular features faded due to the inflow of unlabeled blood; the long delay images are more indicative of tissue perfusion because the signal is primarily in small vessels and tissues.

The ASL activation images (rightmost images in Figs. 1 and 2), produced by subtracting the ASL resting images from the images obtained during the active period, behave very differently with delay. The combined visual stimulation and motor task performance produced detectable flow changes in the primary visual and motor cortices. Although the activation signal intensity decays rather rapidly with increasing post-labeling delay, the spatial distribution of the signal is essentially unaffected. When compared against the resting perfusion images, the absence of bright vascular features is pronounced. This lack of bright vascular features in the short delay images suggests that there is little change in the signal from the labeled blood in these larger vessels. The invariance of the activation signal distribution with delay is more apparent in Fig. 3, where the images have been scaled to correct for T_1 relaxation during the post-labeling delay according to Eq. [1].

The time dependence of the ASL activation signal within the ROIs was analyzed for each subject. In most subjects, the task correlated increase in signal was readily observed in the short delay images, but the lower signal-to-noise ratio at longer delays made this response less apparent (Fig. 4).

The individual subject analyses demonstrated a significant decrease in the transit time and a significant increase in perfusion for both transit time models and regions, Tables 1 and 2. Every subject had a shorter activated transit time and only one subject had a lower activated perfusion according to the distributed transit time model. The resting transit times to the motor cortex were also significantly longer than the transit times to the visual cortex. The mean transit times obtained by fitting to the distributed transit time model were approximately 30% longer than those obtained with the single transit time model. The pseudo-subject data and the corresponding fitted curves are compared in Fig. 5. The theoretical curves are excellent fits to the data. The smoother curves of the distributed transit time model appear to fit the data slightly better than the curves of single transit time model. Formal goodness of fit analysis was avoided because the intersubject and intrasubject noise sources were poorly characterized but the qualitatively good agreement between the theory and experiment provide further support for the validity of the ASL signal model.

The major contribution of transit time changes to the ASL activation signal when short delays are used is emphasized in Fig. 6 where the fractional change in ASL signal due to activation is plotted vs. post-labeling delay. As Eq. [1] shows, the ASL signal is proportional to perfusion. If f is the only quantity to change between the resting and activated conditions, then the fractional change in signal would be independent of post-labeling delay. Instead, the fractional signal increase is two to three times higher at short delays. This additional fractional signal change when short delays are used is the result of transit time change.

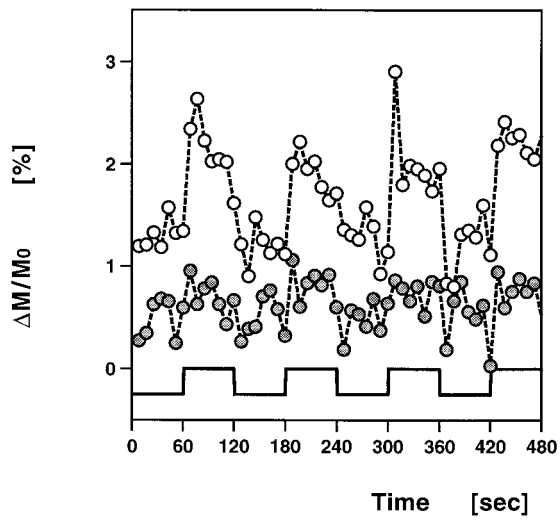

FIG. 4. The fractional signal change in the visual region of interest versus time for a representative subject. Data acquired using a 100-msec post-labeling delay are represented by open circles whereas filled circles correspond to data acquired with a 1200-msec post-labeling delay. The task conditions are indicated by the solid line. Task correlated signal is readily apparent in the 100-msec delay data but the small signal change in the 1200-msec image is more difficult to detect.

Table 1
Fitted Parameters for Eq. [1] (Single Transit Time Model) for Each Subject

Subject	Visual			Motor		
	δ_a Resting (ms)	δ_a Active (ms)	Δf (%)	δ_a Resting (ms)	δ_a Active (ms)	Δf (%)
1	647	536	41	935	904	31
2	840	651	17	948	896	28
3	399	199	10	590	527	16
4	443	297	11	1401	1200	26
5	397	239	13	753	641	11
6	384	334	13	923	779	28
Pseudo	514	360	14	906	739	18
p	0.0007		0.007	0.006		0.0004

The *p* values correspond to single-sided probabilities. The pseudo-subject fits are shown in Fig. 5.

DISCUSSION

Our results demonstrate that quantitative studies of functional activation are possible with a multislice CASL sequence. They also emphasize the important contribution of transit time changes to the CASL activation signal when short post-labeling delays are used. If we had assumed a constant ATT, the activation induced change in perfusion measured with short delays would have been about twice the perfusion change measured with long delays (Fig. 6).

The true perfusion changes derived from the fits are lower than those reported previously with ASL MRI for motor and visual tasks. Buxton et al. (9) reported a 130% flow increase for motor activation whereas Ye et al. (10) reported an average perfusion change of 91%. Visual stimulation induced flow increases of 17 to 35% have been reported by Talagala et al. (11). One reason for our lower perfusion changes may be the use of large regions of interest that were not defined by statistical tests as in Buxton et al. (9) and Ye et al. (10). Averaging of a focal perfusion change over a larger area can dilute the amplitude of the effect. Smoothing of the images with a 15-mm gaussian kernel reduced the perfusion activation to 42% according to Ye et al. (10). Also, the labeling plane in Ye et al. was closer to the imaged slices than our multi-slice experiment allows. Talagala et al. (11) neglected transit time effects. The long duration of our experiment may also have caused a decrease in perfusion due to habituation. Our flashing LED visual stimulus is also known to produce weaker and less reliable activation than the alternating checkerboard pattern used by Talagala et al. (11). Our large ROI results are more comparable to those determined using positron emission tomography: perfusion changes of 30.4 ± 6.5% for motor activation (2) and 31.5 ± 6.2% for visual activation (1). Our finding of a shortened arterial transit time during activation is consistent with the observation of increased arterial flow velocities with functional activation (22,23). Whereas uncertainties in the effects of blood velocity distribution in the blood flow through the carotids and vertebral arteries precludes a definitive measurement of absolute transit times, both models described in this paper indicate that all subjects show a shortening of the transit time during activation for both visual and motor tasks. Our finding of a significant transit time decrease is qualitatively consistent with the report of Buxton et al. (9). Because their results were obtained using pulsed inversion with a slab close to the slice, direct quantitative comparison is not possible.

ASL activation images obtained with short post-labeling delays surprisingly do not display the vascular artifacts and degradation of spatial resolution characteristic of resting ASL images with short delays. The excellent spatial resolution of the transit time induced changes in the ASL activation images suggest that most of the change in transit time results from faster transit through the vessels immediately proximal to the activated region. Because the use of short post-labeling delays does not appear to compromise

Table 2
Fitted Parameters for Eq. [4] (Distributed Transit Time Model) for Each Subject

Subject	Visual			Motor		
	δ_a Resting (ms)	δ_a Active (ms)	Δf (%)	δ_a Resting (ms)	δ_a Active (ms)	Δf (%)
1	851	677	41	1423	1270	24
2	1144	783	11	1378	1183	21
3	350	210	14	738	677	14
4	501	396	11	2391	1511	−6
5	409	236	13	1043	856	8
6	388	377	15	1232	1058	28
Pseudo	584	438	17	1192	1043	21
p	0.009		0.007	0.04		0.02

The *p* values correspond to single-sided probabilities. The pseudo-subject fits are shown in Fig. 5.

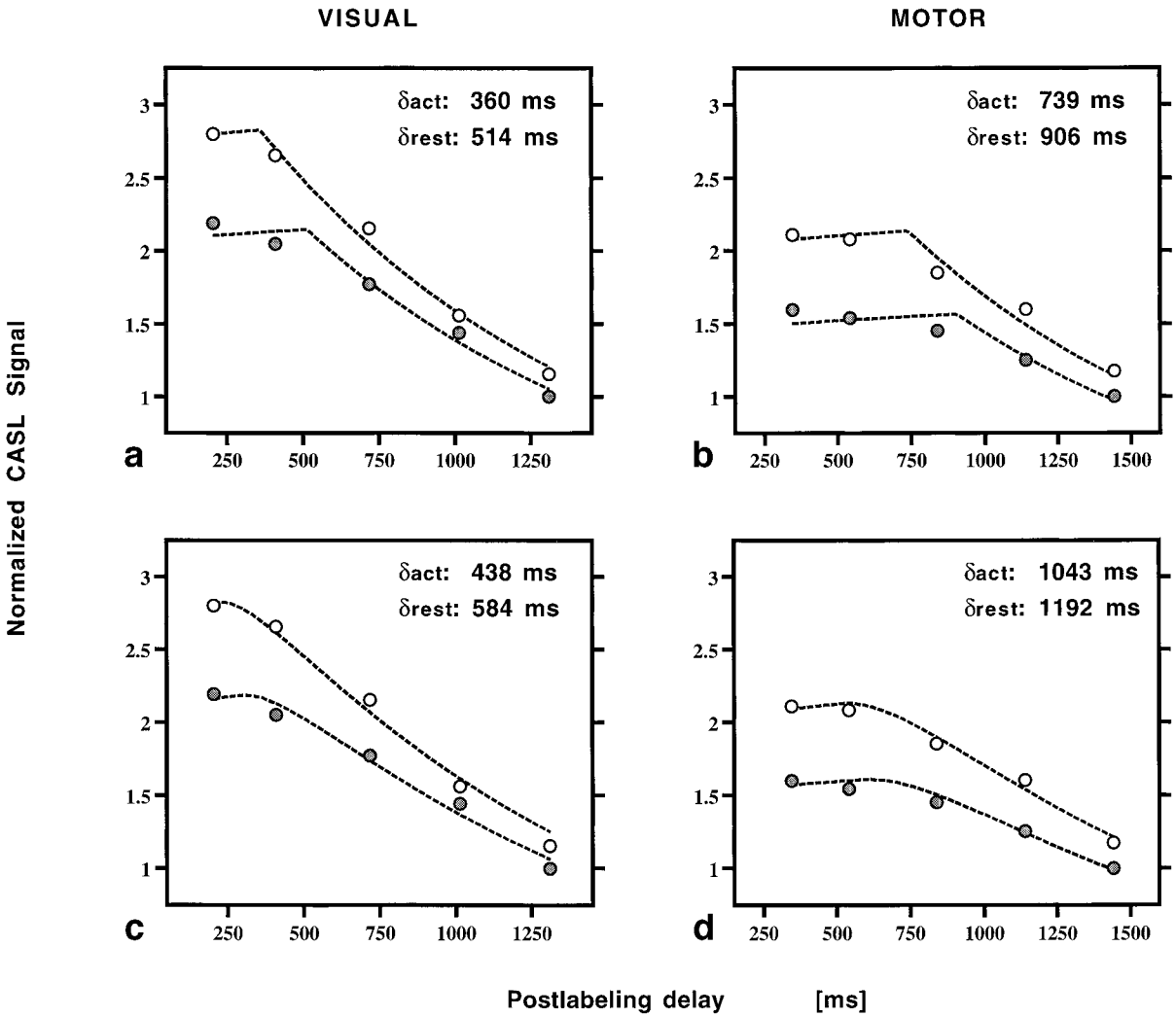

FIG. 5. The dependence of the ASL signal on post-labeling delay. The pseudo-subject averaged ASL signal is shown for both the resting state (filled circles) and the activated state (open circles). The results for the visual cortex region of interest (**a**,**c**), are plotted separately from the results for the motor region (**b**,**d**). The best fit model results are shown using dashed lines. Results using the single transit time model are plotted in **a** and **b**, whereas the results from the distributed transit time model are plotted in **c** and **d**.

spatial resolution and the sensitivity of the short post-labeling delay images to activation is higher, short post-labeling delays may be preferable for ASL activation imaging when quantification of CBF is not required.

The observed decrease in transit time in this study relative to the perfusion increase was unexpectedly large. Doppler ultrasonography of flow velocity changes in large cranial vessels affected by task activation has shown substantial changes in the velocity of the feeding artery (22,23). Nevertheless, a fractional transit time change proportional to the fractional flow change, as indicated in this report, will only arise if the labeled artery supplies only the activated area and if the radii of the supplying arteries do not change. The presence of arterial branches feeding unactivated areas or expansion of the arteries to increase flow will tend to attenuate the transit time change relative to the flow change. We have explored other parameters in our model which could explain the observed signal changes and have found that only changes in the blood T_1 in response to activation can produce comparable signal curves. A 25% decrease in T_1 of blood in the visual regions and a 27% decrease in the motor region can fit the data without any transit time change. Such a T_1 change could occur if the hematocrit of the blood increases during activation. A lower hematocrit is a well accepted phenomena in capillary sized vessels (24) and a proportional relationship between flow and hematocrit has been measured with PET in patients with cerebrovascular disease (25). However, the limited literature in support of a hematocrit change accompanying activation makes this a speculative alternative explanation for our results.

CONCLUSIONS

Transit time decreases contribute significantly to the measured ASL signal changes induced by task activation. Failure to account for these transit time effects will yield spuriously high values for the fractional perfusion increases at short post-labeling delays. Though signal changes resulting from transit time changes could poten-

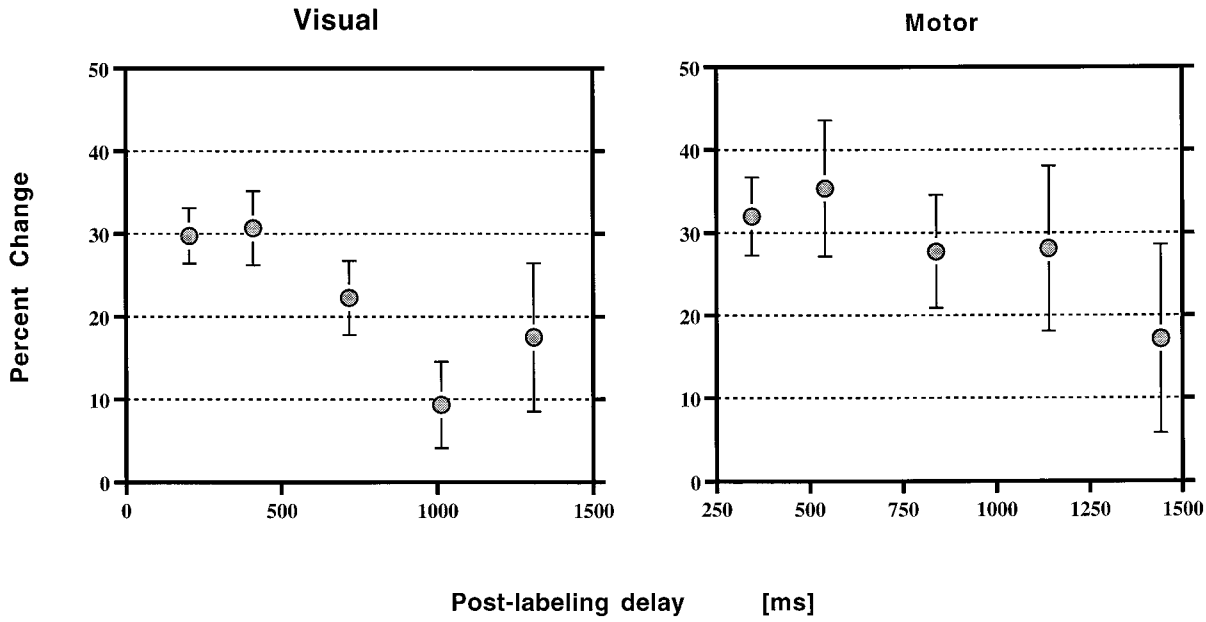

FIG. 6. The percent increase in ASL signal due to activation as a function of the post-labeling delay. Averaged results from both the visual regions and the motor regions are shown. Because the ASL signal change is proportional to perfusion, the percent change should be independent of the delay unless transit time changes are present. The decrease in fractional signal change with post-labeling delay indicates a significant transit time change. Error bars indicate standard deviations ($N = 6$).

tially degrade spatial resolution, we observed no such degradation implying that ASL studies at short post-labeling delay could be preferable when absolute quantification of the magnitude of the perfusion change is not required. Our measurements suggest that fractional transit time changes accompanying activation are approximately equal in magnitude and opposite in sign to fractional perfusion changes.

ACKNOWLEDGMENTS

This work was supported by National Institute of Neurological Disorders and Stroke Grants NS01668 and NS02079 (J.A.D.) and by a grant from the Whitaker Foundation (D.C.A.).

APPENDIX

Our analysis neglected the saturation of labeled blood which may result from imaging of a proximal slice. Such saturation of the labeled blood would artificially decrease the ASL signal intensity in the second slice. The use of spatially interleaved acquisition (slices 1, 3, 5, and 7 acquired before slices 2, 4, 6, and 8) for this study complicates the estimation of the magnitude of this error. Nevertheless, we argue this effect is small for two reasons. First, the initial four slices acquired should be unaffected because these images are acquired at 2-cm spacing every 60 msec. Blood would have to flow at 33 cm/sec just to reach the next slice before it was imaged and considerably faster to build up an effect on ASL image intensity. The average velocities of the cerebral arteries are all less than 70 cm/sec (26) and their paths are also angled and tortuous so the effective velocity from slice to slice will likely be much slower. Second, an estimate of the magnitude of the error in the remaining four slices, elaborated below, suggests a small contribution.

Assuming that blood flows at constant velocity from the labeling plane to the imaged slices, the blood velocity is given by the ratio of the distance to the labeling plane and the transit time. The second lowest slice containing part of the visual region is located 5.1 cm from the labeling plane and the measured transit time was 514 msec. The highest slice containing part of the motor region is 11.5 cm from the labeling plane and the transit time was 906 msec. These results imply a blood velocity of approximately 10 cm/sec. Neglecting the difference between the T_1's of blood and gray matter, the ASL signal is given by

$$S = \frac{2\alpha M_b^0 f}{\lambda}\int_{-\infty}^{0} dt\, \exp\left(\frac{(t - \max(\delta, w))}{T_1}\right).$$

The worst case will occur if the saturated blood from the most inferior slice just finishes entering the slice at t = 0. The saturated blood from an inferior slice will flow into the imaged slice for 80 ms because the slice thickness is 8 mm and the velocity is 10 cm/sec. The saturated blood from the next most inferior slice will have entered 2[cm]/10[cm/sec], or 200 msec, earlier. The fractional error in the signal is then given by

$$Er = (1 - \exp(-80/1100)) \times \sum_{m=1}^{n} \exp(-(m-1)200/1100)$$

where n is the number of slices imaged before the slice under consideration. Only the four first slices saturate blood early enough for it to reach the later slices so n ranges from 1 for the second most inferior slice to 4 for the most superior slice. The worst case fractional errors in the signal are then 7%, 13%, 18%, and 22% for the second, fourth, sixth, and eighth slices, respectively. Because these slices contribute only 30% (40%) of the signal of our visual (motor) ROI, the error in the visual region should be less than 5% and the error in the motor region less than 10%. The effect disappears for long w, as eventually there will be no labeled blood in the saturated slice, thus the fitted transit time will be slightly overestimated.

REFERENCES

1. Fox PT, Raichle ME. Stimulus rate dependence of regional blood flow in human striate cortex, demonstrated by positron emission tomography. J Neurophisiology 1984;51:1109–1120.
2. Ramsey NF, Van Gelderen T, Berman KF, Duyn JH, Frank JA, Mattay VS, Van Horn JD, Esposito G, Moonen CTW, Weinberger DR. Functional mapping of human sensorimotor cortex with 3D BOLD fMRI correlates highly with H2 15O PET rCBF. J Cereb Blood Flow Metab 1996;16:755–764.
3. Chen Q, Siewert B, Bly BM, Warach S, Edelman RR. STAR-HASTE: perfusion imaging without magnetic susceptibility artifact. Magn Reson Med 1997;38:404–408.
4. Crelier GR, Hoge RD, Pike GB. Perfusion-based functional magnetic resonance imaging with single-shot RARE and GRASE acquisitions. Magn Reson Med 1999;41:132–136.
5. Siewert B, Bly BM, Schlaug G, Darby DG, Thangaraj V, Warach S, Edelman RR. Comparison of the BOLD- and EPISTAR-technique for functional brain imaging by using signal detection theory. Magn Reson Med 1996;36:249–255.
6. Kwong KK, Belliveau JW, Chesler DA, Goldberg IE, Weisskoff RM, Poncelet BP, Kennedy DN, Hoppel BE, Cohen MS, Turner R. Dynamic magnetic resonance imaging of human brain activity during primary sensory stimulation. Proc Natl Acad Sci USA 1992;89:5675–5679.
7. Edelman RR, Siewert B, Darby DG, Thangaraj V, Nobre AC, Mesulam M, Warach S. Qualitative mapping of cerebral blood flow and functional localization with echo-planar MR imaging and signal targeting with alternating radio frequency. Radiology 1994;192:513–520.
8. Kim SG. Quantification of relative cerebral blood flow change by flow-sensitive alternating inversion recovery (FAIR) technique: application to functional mapping. Magn Reson Med 1995;34:293–301.
9. Buxton RB, Frank LR, Wong EC, Siewert B, Warach S, Edelman RR. A general kinetic model for quantitative perfusion imaging with arterial spin labeling. Magn Reson Med 1998;40:383–396.
10. Ye FQ, Smith AM, Yang YH, Duyn J, Mattay VS, Ruttimann UE, Frank JA, Weinberger DR, McLaughlin AC. Quantitation of regional cerebral blood flow increases during motor activation: a steady-state arterial spin tagging study. Neuroimage 1997;6:104–112.
11. Talagala SL, Noll DC. Functional MRI using steady state arterial water labeling. Magn Reson Med 1998;39:179–183.
12. Alsop DC, Detre JA. Reduced transit-time sensitivity in noninvasive magnetic resonance imaging of human cerebral blood flow. J Cereb Blood Flow Metab 1996;16:1236–1249.
13. Williams DS, Detre JA, Leigh JS, Koretsky AP. Magnetic resonance imaging of perfusion using spin inversion of arterial water. Proc Natl Acad Sci USA 1992;89:212–216.
14. Maccotta L, Detre JA, Alsop DC. The efficiency of adiabatic inversion for perfusion imaging by arterial spin labeling. NMR Biomed 1997;10: 216–221.
15. Abragam A. Principles of nuclear magnetism. Oxford: Oxford University Press; 1961.
16. Alsop DC, Detre JA. Multi-section cerebral blood flow MR imaging with continuous arterial spin labeling. Radiology 1998;208:410–416.
17. Alsop DC, Detre JA. Reduction of excess noise in fMRI using noise image templates. In: Proceedings of the 5th Annual Meeting of ISMRM, Vancouver, 1997.
18. Vymazal J, Righini A, Brooks RA, Canesi M, Mariani C, Leonardi M, Pezzoli G. T1 and T2 in the brain of healthy subjects, patients with Parkinson disease, and patients with multiple system atrophy: relation to iron content. Radiology 1999;211:489–495.
19. Steen RG, Gronemeyer SA, Kingsley PB, Reddick WE, Langston JS, Taylor JS. Precise and accurate measurement of proton T1 in human brain in vivo: validation and preliminary clinical application. J Magn Reson Imaging 1994;4:681–691.
20. Bryant RG, Marill K, Blackmore C, Francis C. Magnetic relaxation in blood and blood clots. Magn Reson Med 1990;13:133–144.
21. Gomori JM, Grossman RI, Yu-Ip C, Asakura T. NMR relaxation times of blood: dependence on field strength, oxidation state, and cell integrity. J Comput Assist Tomogr 1987;11:684–690.
22. Aaslid R. Visually evoked dynamic blood flow response of the human cerebral circulation. Stroke 1987;18:771–775.
23. Conrad B, Klingelhofer J. Dynamics of regional cerebral blood flow for visual stimuli. Exp Brain Res 1989;77:437–441.
24. Pries AR, Secomb TW, Gaethgens P. Biophysical aspects of blood flow in the microvasculature. Cardiovasc Res 1996;32:654–667.
25. Yamauchi H, Fukuyama H, Nagahama Y, Katsumi Y, Okazawa H. Cerebral hematocrit decreases with hemodynamic compromise in carotid artery occlusion: a PET study. Stroke 1998;29:98–103.
26. Martin PJ, Evans DH, Naylor AR. Transcranial color-coded sonography of the basal cerebral circulation. Stroke 1994;25:390–396.